Design of a Novel Modular Energy Conversion Scheme for DC Offshore Wind Farms

Manex Barrenetxea, Igor Baraia
University of Mondragon
Faculty of Engineering
Arrasate, Spain
mbarrenetxeai@mondragon.edu
ibaraia@mondragon.edu

Igor Larrazabal, Ignacio Zubimendi
Ingeteam Power Technology
Technology
Zamudio, Spain
igor.larrazabal@ingeteam.com
ignacio.zubimendi@ingeteam.com

***Abstract*— Offshore wind farms provide benefits over onshore farms in terms of the amount of generated energy and environmental impact. Cost efficient energy transmission is one of the challenges of those installations. In this context direct connection of parallel connected DC wind turbines to the transmission line is a promising solution. Modular DC-DC converters are an attractive solution for the direct connection of the DC wind turbines to the transmission line. In addition, the phase-shifted full-bridge converter (PSFB) is a good candidate to form simple, efficient and reliable high voltage modular DC-DC converters for offshore DC networks. This paper proposes a novel energy conversion scheme for the direct connection of the DC wind turbines to the transmission line. Design criteria for the phase-shifted full-bridge converter and the medium frequency transformer are described and a modular energy conversion scheme is sized to operate with 10MW offshore wind turbines and 300kV transmission voltage.**

Keywords—DC collection network, modular DC-DC converter, phase-shifted full-bridge converter, medium frequency transformer

I. INTRODUCTION

In European Union, *Europe 2020* strategy, has led to an increase of the installed renewable power capacity. In this context, it is expected that the 15% of the electricity generated in Europe will proceed from wind energy in 2020 [1]. Thereafter, it is expected that the 30% of the total wind power generation will come from offshore wind farms [1]. Due to the steadier and higher speed wind in offshore sites, higher power extraction than in onshore farms is possible. In addition, the lower environmental impact of offshore wind farms allows the installation of larger turbines than in onshore farms [2].

However, the installation of offshore wind farms involves a series of challenges that increases their complexity. Salty, corrosive and humid environment threatens the life expectancy of those installations [3]. In addition, the accessibility to offshore installations for maintenance or reparation works is more difficult than in onshore wind farms. Furthermore, the transmission of the generated energy through submarine cables is challenging. Depending on the distance and the transmitted power, a high voltage alternating current (HVAC) or a high voltage direct current (HVDC) transmission system can be used [4]. As a reference for subsea and underground cable systems, 80 km is generally considered as the boundary distance above which a HVDC transmission system is preferred [5].

If HVAC transmission lines are used, the capacitive behaviour of the long submarine cables increases the amount of circulating reactive current. This leads to additional power cable losses, so, the longer the transmission distance the higher the power losses [5]. On the other hand, with HVDC transmission lines, there is no circulating reactive current. Consequently, better transmission line utilization is achieved [6]. Furthermore, HVDC links require smaller right of ways (power corridors) than their HVAC counterparts due to their smaller diameter and the use of two cables instead of three [7].

Currently, all installed offshore wind farms with HVDC transmission systems have an alternative current (AC) collection network to connect all the wind turbines [8]. Then, the collected energy is transmitted by the HVDC system. In addition to circulating reactive currents, the AC grid collector needs a sizable offshore platform to shelter a bulky AC transformer [9]. This increases installation costs. Recent research has focused on substituting AC collection networks by a direct current (DC) equivalent. The use of DC collection networks may improve overall system efficiency (no reactive currents through the cables) and reduce space requirements (elimination of the bulky line frequency AC transformers) [9].

Although different DC collection systems have been proposed [9-12] the parallel connection of DC wind turbines is promising and provides an effective DC collection network solution [9]. In this layout, all the DC wind turbines are connected in parallel directly to the transmission line. Thus, offshore platforms are no longer required, consequently saving an estimated 15-20% of the total infrastructure costs [9].

The lack of a standard converter that operates as a DC-DC transformer is the main challenge of this proposal. This converter must be able to boost the turbine side low DC voltage up to the level required for transmission. In addition, the DC-DC transformer must compete in terms of reliability and efficiency with the AC transformer.

It has been demonstrated in previous works [13] that the phase-shifted full-bridge converter (PSFB) is a good candidate

to form simple, efficient and reliable high voltage modular DC-DC converters for offshore DC networks.

Thus, in the first part of the paper, a novel modular energy conversion scheme which allows the direct connection of the DC wind turbines to the HVDC transmission line is proposed. In the second part, the design criteria for the main components of the modular energy conversion system are described. Finally, a case study is presented and the required modular converter is designed.

II. Description of the Proposed Modular Energy Conversion Scheme

Fig. 1 shows the proposed modular energy conversion scheme for parallel connected DC collection networks. The energy conversion scheme is composed of several single phase power stacks. Each stack is formed by a single phase H-bridge (HB) rectifier and a modular DC-DC converter with several input-parallel output-series (IPOS) connected DC-DC converters. The IPOS connection of single DC-DC converters avoids the parallel or series connection of switching devices. Thus, the complexity of a single converter design is reduced. Fig. 1 shows the power stacks are series connected to enable direct connection of the wind turbine to the transmission lines. Depending on the number of power stacks and the number of DC-DC converters in each stack, the converter can operate at any input and output voltage level. Additionally, with a large number of DC-DC converters, the proposed modular DC-DC converter can continue delivering full power even if some modules fail (inherent internal fault management against module failure).

In [13] an analysis, comparison and selection of DC-DC converters for the proposed modular energy conversion scheme is presented. Qualitative analysis was used to reduce the pool for choices to between series resonant (SR) and the phase-shifted full-bridge (PSFB) converters. The detailed quantitative comparison of these two converters shows that the phase-shifted full-bridge converter is better suited for the proposed modular energy conversion scheme than the series resonant converter.

In this paper, the design process of the key components of the modular DC-DC converter is described. The minimum number of required converters is calculated and the designs of the PSFB converter and the medium frequency transformer are presented.

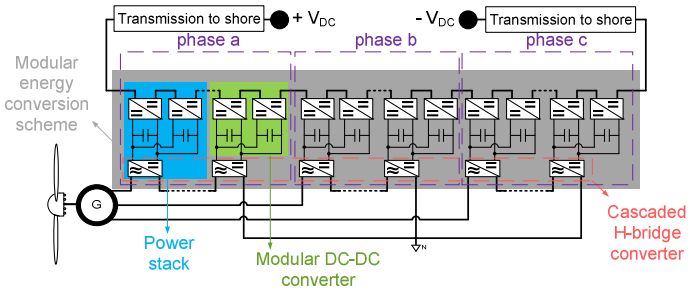

Fig. 1. Proposed modular energy conversion scheme.

III. Design of the Proposed Modular Energy Conversion Scheme

The energy conversion system converts the generator side AC voltage to the transmission side DC voltage. The transmission voltage depends on the transmitted power (wind farm rated power), the transmission line distance, the cable impedance and the expected line efficiency.

A. Number of required power stacks and DC-DC converters

The minimum number of required DC-DC converters depends on the amount of phases (n_ϕ), the transmission voltage (V_{trans}), the voltage rating of the output stage rectifier diodes (V_{diode}) and the considered safety margin for the output stage rectifier diodes (τ). It can be expressed as:

$$N_{DC-DC\min} = n_\phi \cdot ceil\left(\frac{V_{trans}}{n_\phi \cdot V_{diode} \cdot \tau}\right) \quad (1)$$

Once the minimum number of required DC-DC converters is calculated, the number of single phase HB rectifiers ($N_{HB\text{-}\phi}$) per phase and the number of the DC-DC converters connected to each HB ($N_{DC\text{-}DC\_HB}$) are calculated. Each HB with its DC-DC converters forms a power stack, Fig. 1. During normal operation, a failure in several DC-DC converters or a failure in a HB (per phase) can occur, thus, redundant converters are included to continue operating after a failure. If $N_{DC\text{-}DCmin}$ DC-DC converters are available, the DC wind turbine can continue operating. Hence, the number of required HB ($N_{HB\text{-}\phi}$) converters must satisfy this condition:

$$\left(N_{HB-\phi}-1\right)\cdot N_{DC-DC\_HB} \geq {N_{DC-DC\min}}/{n_\phi} \quad (2)$$

The DC bus voltage of each HB converter depends on the generator voltage ($V_{generator}$) and the minimum number of HB converters per phase:

$$V_{bus} = \frac{\sqrt{2}\cdot V_{generator}}{\sqrt{3}\cdot\left(N_{HB-\phi}-1\right)} \quad (3)$$

B. Design of the phase-shifted full-bridge converter

Fig. 2 shows the structure of the PSFB converter. The input DC bus voltage is inverted and applied to the primary of the medium frequency transformer (MFT). This voltage is rectified and filtered in the output stage. The phase-shifting [10] modulation scheme enables zero voltage switching (ZVS) turn on. In addition, this modulation scheme leads to negligible switching losses in the diode rectifier. In order to avoid transformer saturation, the control scheme must guarantee that the average voltage applied to MFT is zero (no DC injection).

Fig. 3 shows typical current and voltage waveforms of this converter. From those waveforms, the equations used to design the converter are deduced.

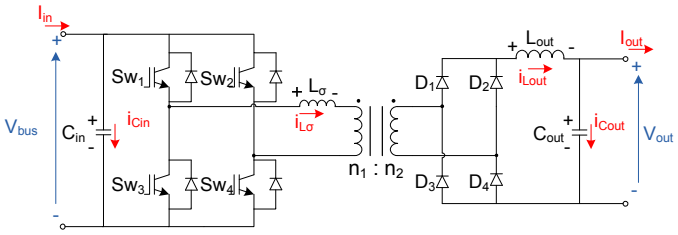

Fig. 2. Phase-shifted full-bridge converter.

The output voltage of each DC-DC converter depends on the transmission voltage (V_{trans}) and the minimum number of DC-DC converters:

$$V_{out} = \frac{V_{trans}}{n_{\phi} \cdot (N_{HB-\phi} - 1) \cdot N_{DC-DC\_HB}} \tag{4}$$

The transformer turn ratio (n_1, n_2) is calculated taking into account the input DC bus voltage (V_{bus}) and the effective duty cycle (δ_{eff}), Eq. (5).

$$\frac{n_2}{n_1} = \frac{V_{out}}{2 \cdot V_{bus} \cdot \delta_{eff}} \tag{5}$$

From Eq. (6), the effective duty cycle depends on the duty cycle (δ), the leakage inductance (L_σ), the switching frequency (f_{sw}), the input power (P_{in}) and the input voltage (V_{bus}). If the transformer has a low leakage inductance, a high effective duty cycle even with high switching frequencies can be achieved.

$$\delta_{eff} = \delta - L_\sigma \cdot \left(\frac{2 \cdot P_{in} \cdot f_{sw}}{V_{bus}^{\,2}} \right) \tag{6}$$

From Fig. 3 (b), the output filter inductance (L_{out}) is based on the desired output current ripple (Δi_{out}) as:

$$L_{out} = \frac{V_{out} \cdot (0.5 - \delta_{eff})}{f_{sw} \cdot \Delta i_{out}} \tag{7}$$

From Fig. 3 (c), the output filter capacitance (C_{out}) is based on the desired output voltage ripple (Δv_{out}) and the output current ripple (Δi_{out}) as:

$$C_{out} = \frac{\Delta i_{out}}{16 \cdot f_{sw} \cdot \Delta v_{out}} \tag{8}$$

The input capacitance (C_{in}) has been calculated considering the instantaneous active power through the single phase HB rectifier. Compared to a three phase rectifier, single phase rectifiers have a second harmonic current component that leads to higher DC bus capacitance requirements.

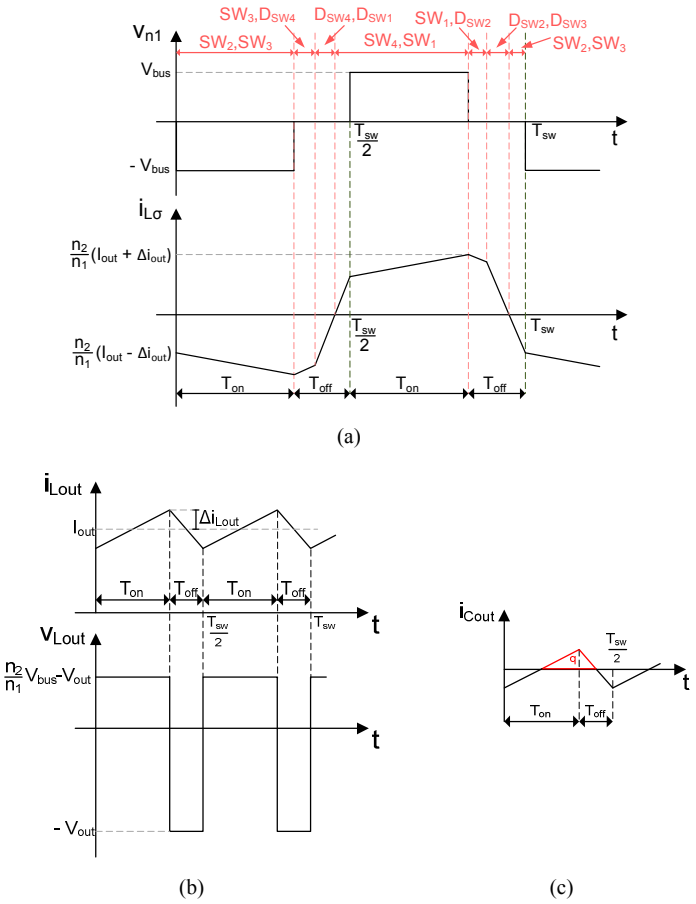

Fig. 3. Current and voltage waveforms of the a) primary winding of the transformer, b) output side inductor and c) charges through the output capacitor.

$$C_{in} \approx \frac{V_{\max HB} \cdot I_{\max HB}}{4 \cdot \pi \cdot V_{bus} \cdot \Delta v_{cin} \cdot f_{generator}} \tag{9}$$

Average conduction power losses (P_{cond}) depends on the semiconductor switch on-state resistance and threshold voltage drop (r_d, V_{th}) and the current flow in the switching device (I_{rms}, I_{ave}).

$$P_{cond} = r_d \cdot I_{rms}^{\,2} + V_{th} \cdot I_{ave} \tag{10}$$

TABLE I. SIMPLIFIED CURRENT EXPRESIONS FOR THE AVERAGE CONDUCTION POWER LOSS CALCULATION

	Average current (I_{ave})	***RMS current (I_{rms})***
IGBT	$I_{out} \cdot \frac{n_2}{n_1} \cdot \left(\lambda - \frac{3 \cdot n_2 \cdot I_{out} \cdot L_\sigma}{2 \cdot n_1 \cdot V_{bus} \cdot T_{sw}} \right)$	$I_{out} \cdot \frac{n_2}{n_1} \cdot \sqrt{\lambda - \frac{5 \cdot I_{out} \cdot L_\sigma \cdot n_2}{3 \cdot n_1 \cdot V_{bus} \cdot T_{sw}}}$
Freewheel diodes	$I_{out} \cdot \frac{n_2}{n_1} \cdot \left(\gamma + \frac{n_2 \cdot I_{out} \cdot L_\sigma}{2 \cdot n_1 \cdot V_{bus} \cdot T_{sw}} \right)$	$I_{out} \cdot \frac{n_2}{n_1} \cdot \sqrt{\gamma + \frac{I_{out} \cdot L_\sigma \cdot n_2}{3 \cdot n_1 \cdot V_{bus} \cdot T_{sw}}}$
Output stage diodes	$I_{out} \cdot \left(\frac{1}{2} - \frac{2 \cdot I_{out} \cdot L_\sigma \cdot n_2}{n_1 \cdot V_{bus} \cdot T_{sw}} \right)$	$I_{out} \cdot \sqrt{\frac{1}{2} - \frac{2 \cdot I_{out} \cdot L_\sigma \cdot n_2}{n_1 \cdot V_{bus} \cdot T_{sw}}}$

From Table 1, the currents circulating through the IGBTs, freewheel diodes and the output rectifier diodes are calculated. T_{sw} is the switching period and the parameters λ and γ depends on the position of the switch in the converter. The current circulating from Sw_1 and Sw_3 differs from the current circulating from Sw_2 and Sw_4 (same can be applied to their freewheel diodes, Fig. 3(a)). Therefore, for Sw_1-Sw_3 and their respective freewheel diodes $\lambda=\delta$ and $\gamma=(0.5-\delta)$ is considered and in turn, for Sw_2-Sw_4 and their respective freewheel diodes $\lambda=0.5$ and $\gamma=0$ is considered.

Average switching losses depends on the switched current (i_{sw}), switched voltage (v_{sw}), switching frequency (f_{sw}), and the energy loss characteristic provided by the manufacturer (A_{sw}, B_{sw}, C_{sw}) for the 100FIT test voltage (V_{100FIT}).

$$P_{sw} = \sum_{n=1}^{x} \frac{v_{sw}(n)}{V_{100FIT}} \cdot \left(A_{sw} \cdot i_{sw}(n)^2 + B_{sw} \cdot i_{sw}(n) + C_{sw}\right) \cdot f_{sw} \quad (11)$$

Switching losses of rectifier diodes and turn on losses of IGBTs are negligible. Eq. (12) and Eq. (13) shows respectively the IGBT turn off currents and voltages, where $\rho=\Delta i_{out}$ for Sw_2-Sw_4 and $\rho=0$ for Sw_1-Sw_3.

$$I_{SwIGBT} \approx \left(I_{out} + \rho\right) \cdot \frac{n_2}{n_1} \quad (12)$$

$$V_{SwIGBT} \approx V_{bus} \quad (13)$$

C. Medium frequency transformer design

The medium frequency transformer is a key component of the DC-DC converter. The transformer must be designed to provide required galvanic isolation and voltage gain. High efficiency and low volume requirements are also mandatory. Fig. 4 shows the procedure followed to design the MFT.

First, the **operational specifications** must be defined. The transmission voltage and the input DC voltage define the required insulation voltage and the turn ratio. The current circulating through the transformer defines the cross sectional area of the windings. The switching frequency of the DC-DC converter has influence on the power losses and the core cross sectional area.

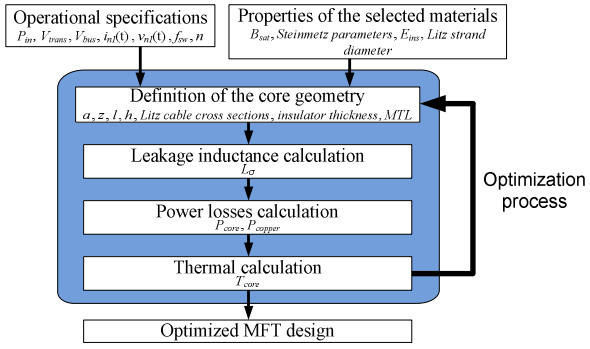

Fig. 4. Medium frequency transformer design flowchart.

Proper core, insulator and conductor **materials must be chosen** to construct the transformer. Amorphous and nanocrystalline materials are attractive due to their high saturation fluxes (about 1.2T) and low specific losses [14]. A high saturation flux reduces the core cross sectional area, Eq. 14.

Despite the cost of Litz cables is higher than conventional cables, the skin and proximity effects in Litz cables are smaller. The parasitic currents caused by skin and proximity effects increases with the frequency leading to additional power losses. Thus, Litz cables are preferred to construct MFTs [15]. Dry-type potted insulators as EPOXY or Micares are suitable insulator materials due to their high dielectric strengths, 16 kV/mm and 8-24 kV/mm respectively [14]. Thus, high voltage differences are withstood in short distances.

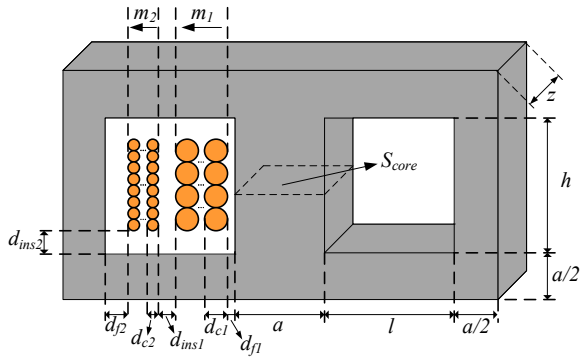

Fig. 5. Medium frequency transformer geometry.

For high-voltage low-current applications shell-type core is the best solution [16]. Fig. 5 shows the **core geometry** of the designed MFT. The core cross sectional area is given by Eq. 14, where B_{sat} is the core saturation flux and ζ is the safety margin considered for the saturation flux (typically 0.1-0.2 [14]).

$$S_{core} = \frac{V_{bus} \cdot \delta_{eff}}{2 \cdot f_{sw} \cdot n_1 \cdot B_{sat} \cdot (1-\zeta)} \quad (14)$$

Litz cable's cross sectional area is defined by the *rms* current (I_{rms}) and the maximum allowable current density (J_n), which is about 1.7-2 A/mm^2 for naturally cooled transformers [15].

$$S_{cable} = \frac{I_{rms}}{J_n} \quad (15)$$

The core geometry can be defined as shown in Eq. 16, Eq. 17 and Eq. 18, where m_1 and m_2 are the number of primary and secondary side layers respectively, d_{c1} and d_{c2} are the diameters of the primary and the secondary side Litz cables respectively and d_{ins1}, d_{ins2}, d_{f1}, d_{f2} are insulation distances.

$$a = \frac{S_{core}}{z} \quad (16)$$

$$l = m_1 \cdot d_{c1} + m_2 \cdot d_{c2} + d_{ins1} + d_{f1} + d_{f2} \quad (17)$$

$$h = \frac{(n_1 + 1)}{m_1} \cdot d_{c1} + 2 \cdot d_{ins2} \quad (18)$$

Thus, winding's mean turn length, core volume and whole transformer's volume are defined by Eq. 19, Eq. 20 and Eq. 21 respectively. d_{f1} is the required insulation distance between the primary winding and the core.

$$MTL = 2 \cdot \left(a + z + \pi \cdot \left(\frac{l - d_{ins1}}{2} + d_{f1} \right) \right) \quad (19)$$

$$V_{core} = 2 \cdot S_{core} \cdot (h + l + a) \quad (20)$$

$$V_{transf} = 2 \cdot (2 \cdot l + z) \cdot (h + a) \cdot (l + a) \quad (21)$$

The **leakage inductance** for non interleaved windings is expressed as follows:

$$L_\sigma = \frac{{n_1}^2 \cdot \mu_0 \cdot MTL}{h} \cdot \left(\frac{m_1 \cdot d_{c1}}{3} + \frac{m_2 \cdot d_{c2}}{3} + d_{ins1} \right) \quad (22)$$

Eq. 23 shows the improved generalized Steinmetz equation (IGSE) for rectangular shape voltages, used for the core **power losses calculation**. K, α and β are the Steinmetz parameters of the selected core [15].

$$P_{core} = 2^{2 \cdot \beta + 1} \cdot k_i \cdot {f_{sw}}^{\alpha} \cdot (B_{sat} \cdot (1 - \zeta))^{\beta} \cdot {\delta_{eff}}^{\beta - \alpha + 1} \quad (23)$$

$$k_i = \frac{K}{2^{\beta+1} \cdot \pi^{\alpha-1} \cdot \left(0.2761 + \frac{1.7061}{\alpha + 1.354} \right)} \quad (24)$$

The skin and proximity effects increases the copper losses. These losses are calculated taking into account each of the current harmonics (I_i) and each cable's DC resistance (Eq. 25) as well as Dowell's resistance factor (Eq. 26) [15]. Thus, Eq. 27 defines the power losses for round cables with small penetration ratios, where σ is the conductivity of the copper ($5.688 \cdot 10^7$ $(\Omega \cdot m)^{-1}$ at 25ºC), μ_0 and μ_r are the vacuum permeability ($4\pi \cdot 10^{-7}$ N/A^2) and copper's relative permeability (0.999994) respectively. In addition, for each winding's (primary or secondary) Litz cable must be considered: the number of turns (N), mean turn length (MTL_X), number of layers (m_X), number of strands (n_s), radius of the strand (r_{str}) and the packing factor (pf).

$$R_{DC} = \frac{N \cdot MTL_X}{\pi \cdot n_s \cdot \sigma \cdot {r_{str}}^2} \quad (25)$$

$$F_r = 1 + \frac{\left(\pi \cdot {r_{str}}^2 \cdot f_{sw} \cdot \mu_0 \cdot \mu_r \cdot \sigma \right)^2}{96} \cdot \left(\frac{1}{3} + \frac{\pi^2 \cdot n_s \cdot pf}{2} \cdot \left(\frac{24}{\pi^2} + 16 \cdot m_X - 1 \right) \right) \quad (26)$$

$$P_{copper} = \sum_i \left(\left(\frac{I_i}{\sqrt{2}} \right)^2 \cdot R_{DC} \cdot F_r \right) \quad (27)$$

Maximum surface temperature has been limited to 100ºC [15]. The surface **temperature calculation** has been carried out following the approach proposed in [17], Eq. 28, where ΔT is the temperature rise of the transformer and S_T the total surface area of the transformer.

$$\Delta T = \left(\frac{P_{core} + P_{copper}}{S_T} \right)^{0.833} \quad (28)$$

A genetic algorithm has been used to optimize the design process and find the best trade-off between the transformer volume and its efficiency, Fig.4.

IV. CASE STUDY

In average, current offshore wind farms are rated at 340 MW and are located up to 70 km from shore [9], [18]. 3-5 MW wind turbines can be found in those installations. In the near future, bigger wind farms farther from the cost are expected [19]. A 500 MW offshore wind farm located at 100 km from shore with 10MW-6.6kV wind turbine generators has been designed to get a picture of the proposed wind farm scheme. The considered transmission cable resistance is 0.009 Ω/km [20]. As observed in Fig. 6 (a), a 300 kV transmission voltage is required to achieve an efficiency of 99% in the transmission line.

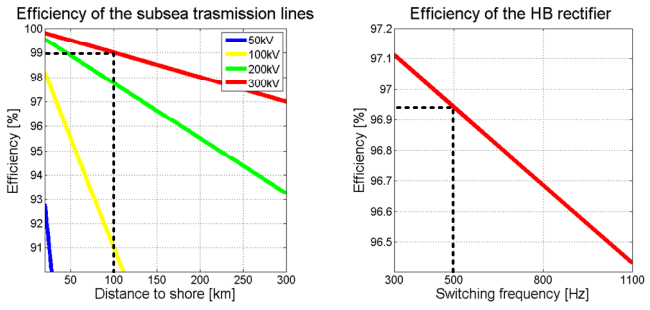

(a) (b)

Fig. 6. Efficiencies of the a) transmission lines and b) HB rectifiers.

6.5 kV (V_{100FIT} = 3.6 kV) diodes have been considered in the output stage rectifier, 1.7kV-150A IGBTs for the input stage of the DC-DC converter and 1.7kV-1200A for the rectifier HB converter. A nanocrystalline core has been used in the MFT and EPOXY was considered as insulator material.

From Table 2, the energy conversion scheme needs 21 power stacks. Each power stack has 1 HB + 5 DC-DC converters. Such amount of DC-DC converters leads to low power DC-DC converters and allows the operation at medium frequency. As expected, this frequency leads to low volume requirements of passive elements [6].

TABLE II. PROPOSED MODULAR CONVERSION SCHEME FOR A 500MW - 300KV TRANSMISSION SYSTEM

Total number of power stacks				21
Total number of DC-DC converters				105
Number of power stacks per phase				7
Number of DC-DC converters per phase				35
Number of DC-DC converters per power stacks				5
Number of redundant power stacks per phase				1
Power of each DC-DC converter				111.1 kW
Input voltage of each DC-DC converter (V_{bus})				916 V
Characteristics of the phase-shifted full-bridge converter				
f_{sw}	***C_{in}***	***C_{out}***	***L_{out}***	***Efficiency***
1.4 kHz	5.971 mF	179.87 nF	61.98 mH	99.09 %
Characteristics of the medium frequency transformer				
Leakage inductance L_σ	***Single transformer volume***	***Total volume for 10 MW***	***Efficiency***	
68.068 μH	42.78 dm^3	4492.2 dm^3	99.78 %	
Efficiency of the transmission system				
HB rectifier	***DC-DC converters***	***Transmission cables***	***Onshore inverter***	***Total efficiency***
96.94 %	98.88 %	99 %	98.2 % [21]	93.18 %

The whole transmission system (HB + DC-DC + Transmission line + Onshore inverter) has been designed to achieve a minimum efficiency of 93.18%. As shown in Fig. 6 (b), the switching frequency of the rectifier HB has been limited to 500Hz to keep switching losses low. This way, the desired efficiency has been achieved. Due to the number of voltage levels, the generator side voltage quality has not been penalized.

V. CONCLUSION

In this paper a novel modular energy conversion scheme for offshore wind farms has been presented and designed. Its high modularity allows the operation at any generator and transmission voltage using standard power stacks. In addition, redundant stacks can be added to increase the reliability of the converter.

A key component of the proposed conversion scheme is the DC-DC converter. A thorough design procedure of the phase-shifted full-bridge converter and the medium frequency transformer has been presented. This design procedure has been applied to a 500MW wind farm located at 100 km from the coast.

Future works will be focused on the control and reliability issues of the proposed energy conversion structure. Also, its cost will be evaluated and compared with existing solutions.

REFERENCES

[1] "EU energy, transport and greenhouse gas emissions trends to 2050," ed. Brussels: European Commission, 2013.

[2] B. Wu, Y. Lang, N. Zargari, and S. Kouro, Power Conversion and Control of Wind Energy Systems: Wiley, 2011.

[3] K. Fischer, T. Stalin, H. Ramberg, J. Wenske, G. Wetter, R. Karlsson, et al., "Field-Experience Based Root-Cause Analysis of Power-Converter Failure in Wind Turbines," Power Electronics, IEEE Transactions on, vol. 30, pp. 2481-2492, 2015.

[4] B. W. Williams, Principles and Elements of Power Electronics. Devices, Drivers, Applications, and Passive Components, 2006.

[5] M. Zubiaga, G. Abad, J. A. Barrena, S. Aurtenetxea, and A. Carcar, Energy Transmission and Grid Integration of AC Offshore Wind Farms: InTech, 2012.

[6] M. R. Islam, Y. Guo, and J. Zhu, "A review of offshore wind turbine nacelle: Technical challenges, and research and developmental trends," Renewable and Sustainable Energy Reviews, vol. 33, pp. 161-176, 2014.

[7] K. Johannesson, A. Gustafsson, J. Karlstrand, and M. Jeroense, "HVDC Light Cables for long distance grid connection," presented at the European Offshore Wind Conference, Stockholm, Sweden, 2009.

[8] N. Holtsmark, H. Bahirat, M. Molinas, B. Mork, and H. Hoidalen, "An All DC Offshore Wind Farm with Series-Connected Turbines: An Alternative to the Classical parallel AC Model?," Industrial Electronics, IEEE Transactions on, vol. 60, pp. 2420-2428, 2013.

[9] J. Pan, S. Bala, M. Callavik, and P. Sandeberg, "DC Connection of Offshore Wind Power Plants without Platform," presented at the 13th Wind Integration Workshop, Berlin, 2014.

[10] L. Max, "Design and Control of a DC Collection Grid for a Wind Farm," Ph. D Thesis, Department of Energy and Environment, Charlmers University of Technology, Göteborg, 2009.

[11] S. Lundberg, "Wind farm configuration and energy efficiency studies - Series DC versus AC layouts," Ph.D Thesis, Department of Electric Power Engineering, Chalmers University of Technology, Göteborg, 2006.

[12] C. Meyer, "Key Components for Future Offshore DC Grids," Ph. D Thesis, Faculty of Electrical Engineering and Information Technology, RWTH Aachen University, Aachen, 2007.

[13] M. Barrenetxea, I. Baraia, I. Larrazabal, I. Zubimendi, G. P. Adam, and B. W. Williams, "Analysis, Comparison and Selection of DC-DC Converters for a Novel Modular Energy Conversion Scheme for DC Offshore Wind Farms," in EUROCON - International Conference on Computer as a Tool 2015, 2015 IEEE.

[14] G. Ortiz, J. Biela, and J. W. Kolar, "Optimized design of medium frequency transformers with high isolation requirements," in IECON 2010 - 36th Annual Conference on IEEE Industrial Electronics Society, 2010, pp. 631-638.

[15] I. Villar, "Multiphysical Characterization of Medium-Frequency Power Electronic Transformers," Ph. D Thesis, Swiss Federal Institute of Technology in Lausanne EPFL, Lausanne, 2010.

[16] A. Bediaga, "Optimal Design of Medium Frequency High Power Converters," Ph. D thesis, Swiss Federal Institute of Technology in Lausanne EPFL, Lausanne, 2014.

[17] G. Orenchak, "Estimating temperature rise of transformers," Power Electronics Technology, vol. 30, pp. 14-22, July 2004.

[18] "Offshore Wind Toward 2020 - On the pathway to cost competitiveness," Roland Berger Strategy Consultants , 2013.

[19] T. Ackermann, Wind Power in Power Systems: Wiley, 2005.

[20] N. B. Negra, J. Todorovic, and T. Ackermann, "Loss evaluation of HVAC and HVDC transmission solutions for large offshore wind farms," Electric Power Systems Research, vol. 76, pp. 916-927, 2006.

[21] P. Hui, T. Guangfu, and H. Zhiyuan, "Evaluation of losses in VSC-HVDC transmission system," in Power and Energy Society General Meeting - Conversion and Delivery of Electrical Energy in the 21st Century, 2008 IEEE, 2008, pp. 1-6.